Continuous strain bursts in crystalline and amorphous metals during plastic deformation by nanoindentation

H. Li, A.H.W. Ngan,[a] and M.G. Wang
Department of Mechanical Engineering, The University of Hong Kong, Hong Kong, People's Republic of China

(Received 4 April 2005; accepted 8 August 2005)

Using depth-sensing indentation with sub-nanometer displacement resolution, the plastic deformation of a range of materials, including a metallic glass, amorphous selenium, Ni_3Al, pure Nb, Al, Cu, and Zn metals, and an Al-Mg alloy, has been investigated at room temperature. In amorphous selenium, even the sub-nanometer displacement resolution of the nanoindentation technique cannot reveal any strain burst during deformation at room temperature. In all other metals studied, what may appear to be smooth load-displacement curves at macroscopic scale during indentation deformation in fact turn out to consist of a continuous series of random bursts of the nanometer scale. The occurrence probability of the bursts is found to decrease at increasing burst size. In all of the crystalline metals and alloys studied, the size distribution of the strain bursts seems to follow an exponential law with a characteristic length scale. The absence of the self-organized critical behavior is likely a result of the small size of the strained volume in the nanoindentation situation, which gives rise to a constraint of a characteristic strain. In the metallic glass sample, due to the limited range of the burst sizes encountered, whether the deformation bursts follow an exponential or a power-law behavior corresponding to self-organized criticality is inconclusive. From a theoretical viewpoint based on the Shannon entropy, the exponential distribution is the most likely distribution at a given mean burst size, and this is thought to be the reason for its occurrence in different materials.

I. INTRODUCTION

Many natural and artificial phenomena, including earthquakes, avalanches in flowing sand piles, fluctuations in commodity prices, and so on, have been found to exhibit self-organized critical (SOC) behavior.[1,2] The SOC behavior is likely to arise in an externally driven physical system involving a large number of interacting objects with an infinite interaction length. If locks that may arise from such interactions are overcome, bursts or avalanches of a wide spectrum of sizes but without any characteristic length or time scale are induced. A characteristic feature of SOC behavior is that the probability density F of the size Ψ of these catastrophic events typically follows a power-law distribution pertinent to fractals

$$F(\Psi) \sim \Psi^{-k} \quad , \tag{1}$$

where k is a dimensionless constant.

The deformation of crystals with significant intrinsic or extrinsic resistance to dislocation motion is well known to be a discontinuous process with discrete strain bursts. De Hosson et al.[3] measured the jump distances of dislocations in solid-solution hardened Al-Zn alloys using a nuclear magnetic resonance technique and found that these jumps exhibit a wide spectrum of sizes. Miguel et al.[4] measured the acoustic emissions during slow deformation of ice crystals and found that larger emissions followed a power-law spectrum of the form given by Eq. (1). The main reason why the SOC behavior can be observed in single crystals of ice is that long-range elastic interactions between moving dislocations are not shielded by obstacles such as solutes or forest dislocations, so that the correlation length of dislocation jamming is very large. Any kind of obstacles to dislocation motion other than dislocation jamming is expected to hinder the occurrence of the SOC behavior. On a related issue, Häfner et al.[5] discovered that dislocations in Cu following deformation arrange themselves into fractal patterns, in which the dislocations form cells with sizes obeying the power-law distribution in Eq. (1). These authors developed a model of dislocation patterning, based on the local balance between dislocation generation, annihilation, and growth, which predicts fractal patterning to occur when the noise level is high enough.[6]

[a]Address all correspondence to this author.
e-mail: hwngan@hku.hk
DOI: 10.1557/JMR.2005.0379

Recently, Ngan[7] developed another model in which pattern formation is governed by both energetics and noise, and fractal geometry is again predicted to occur at high enough noise levels.

In the present study, we use the nanoindentation technique to investigate the strain bursts during continuous deformation of a wide range of metals. The nanoindentation technique provides sub-nanometer displacement resolution and is therefore a convenient tool to probe the occurrence of bursts during deformation. In this study, we used a metallic glass, and a range of crystalline metals and alloys, to investigate the universality of the observed scaling behavior of the deformation bursts.

II. EXPERIMENTAL

In the present work, the deformation behavior during nanoindentation of a range of metallic materials representing different structures was investigated. The details of the materials used are summarized as follows:

(i) A metallic glass sample was supplied by Dr. S.H. Shek of the City University of Hong Kong. Its composition was $(Zr_{63}Ni_{10}Cu_{16}Al_{11})$-Be, the ratios between the heavier elements were determined by energy-dispersive x-ray analysis using a LEO field-emission scanning electron microscope (SEM). The x-ray diffraction as shown in Fig. 1(a) using a Bruker D8 Advance Series 2 XRD system (Bruker AXS GmbH, Karlsruhe, Germany) verified its amorphous structure.

(ii) An amorphous selenium sample was prepared by first melting 99.999% selenium pellets at 300 °C, and then pouring the liquid selenium into a hole in a cylindrical brass block for quenching. The brass with the selenium sample was mechanically polished sequentially on 400- and 800-grit silicon carbide abrasive papers, 6- and 1-μm diamond slurry, and finally finished in a 0.3-μm alumina solution. The x-ray diffraction analysis as shown in Fig. 1(b) revealed that the structure of the sample was amorphous.

(iii) A Ni_3Al(Cr) single crystal was grown by the Bridgeman method. The composition of this material is Ni-75, Al-16.7, Cr-8, and B-0.3 in at.%. The crystal was homogenized at 1250 °C for 120 h in a vacuum better than 10^{-6} Torr followed by furnace cooling. A specimen button with (111) direction was cut and electropolished in a solution containing 10% perchloric acid in ethanol to remove any mechanical deformation layer.

(iv) A 99.99% pure polycrystalline niobium specimen was annealed for 20 days at 1200 °C in a vacuum of approximately 10^{-5} Torr, followed by furnace cooling to room temperature. The resulted grain size is 300–700 μm. The annealed sample was mechanically ground using 600-grade emery paper and then electropolished for 2–5 min in a solution containing 1 part of HF and 9 parts of H_2SO_4 in volume.

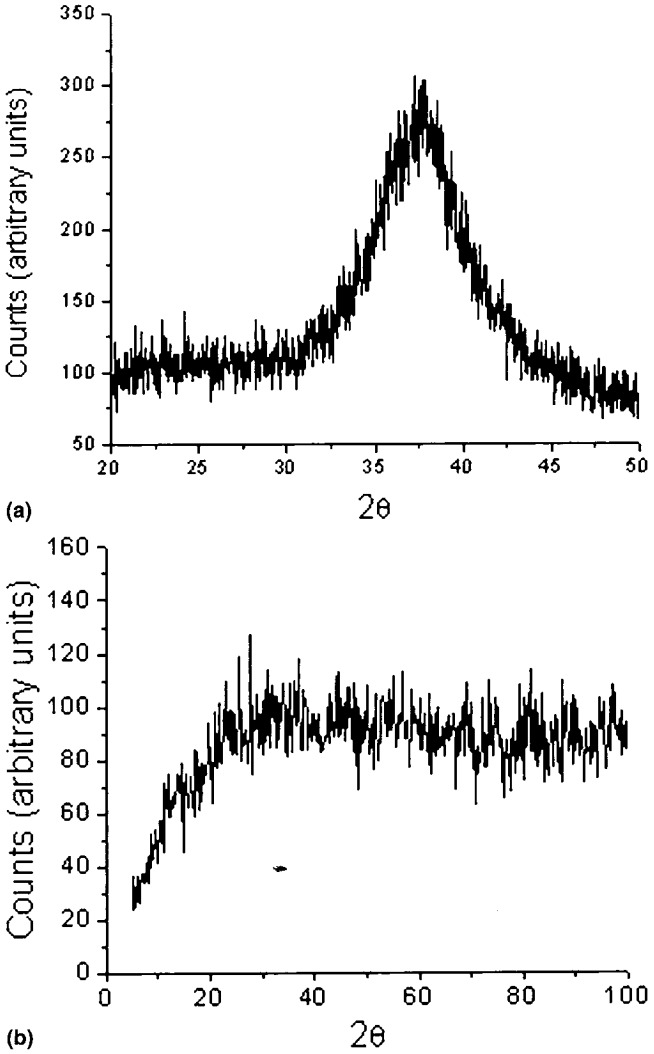

FIG. 1. XRD pattern for (a) $(Zr_{63}Ni_{10}Cu_{16}Al_{11})_{1-x}Be_x$ metallic glass and (b) amorphous selenium.

(v) A 99.99% polycrystalline copper sample was annealed for 5 h at 800 °C in a vacuum better than 10^{-6} Torr, resulting in a grain size larger than 300 μm. The specimen was carefully ground with 600-grade emery paper, followed by polishing with 5- and 1-μm diamond suspension. The specimen was then electropolished for about 30 s to remove any deformation layer on the surface using an electrolyte containing two parts of orthophosphoric acid and one part of distilled water at a voltage of 2.6 V at room temperature.

(vi) A 99.99% pure polycrystalline zinc sample was annealed for 4 h at 280 °C in a vacuum better than 10^{-6} Torr, and the final grain size was larger than 400 μm. The specimen was then mechanically polished down to 1 μm surface finish and finally electropolished in 10% (by volume) $HClO_4$ in CH_3COOH.

(vii) A polycrystalline Al sample (>99.99% pure) was in the as-cast state, polycrystalline state. It was first mechanically polished to 1 μm followed by etching in

NaOH solution and electropolishing in an electrolyte containing 10% perchloric acid in alcohol. Such a process produced a mirror surface with grain size of about 800 μm.

(viii) An Al-5%Mg (by weight) alloy sample with composition listed in Table I was annealed at 500 °C for 1 h, followed by quenching in water. It was then electropolished in a solution containing 6% perchloric acid, 80% ethanol, and 14% distilled water to mirror surface for indentation.

In this work, indentation tests were carried out at room temperature on either a nanoindentation system composing of a Hysitron® transducer mounted on a Thermomicroscopes® scanning probe microscope, or a nanohardness tester supplied by CSM Instruments SA in Switzerland. These two systems represent different load ranges and data sampling rates, but both have subnanometer displacement resolutions. The Hysitron system can apply loads up to 10 mN with higher locating capability of the indentation point, and its maximum number of sampling points in one run is 8000, implying that the sampling rate is more frequent in the time domain for shorter tests. The CSM nanoindenter was used due to its much higher load and displacement range when compared with the Hysitron machine. Its sampling rate is fixed at 10 points per second, regardless of the test duration. The typical loading sequence in this work consisted of a simple load ramp with a holding period at a small load for the measurement of drift rate, as shown in Fig. 2. A range of loading rates spanning at least 2 orders of magnitude was used in most cases to examine any strain rate effects. The peak loads were not necessarily identical for different materials. The test at each load specification was repeated 10 times or more to generate enough statistical information. When testing polycrystalline specimens, the indentation points were always well within the interior of selected grains of sizes much larger than the indent sizes, so that the measurements were effectively on single crystals. This was possible since the grain sizes of the polycrystalline samples used were all several hundreds of microns, but the typical size of an indent was of the order of one micrometer.

III. RESULTS AND ANALYSES

A. Metallic glass

Serrated flow, which has been observed by many previous researchers,[8–12] is also found to occur in the present nanoindentation experiments on our metallic glass sample. These are in the form of random bursts of various sizes along the loading curve as shown in Fig. 3. While the occurrence of the majority of the bursts is random, it is found that a major burst, with much larger excursion than others in the same run, always occurs at a depth of about 500 nm for all the loading rates studied, and its size generally increases at lower loading rates. The major burst that consistently occurred at ~500 nm is likely to result from some characteristic event, such as the formation of a macroscopic crack in the sample, and in what follows, we focus instead on the smaller, random bursts along the entire load-displacement curve. As shown in Fig. 4, the load-displacement curves at different loading rates studied overlap quite well when their origins are aligned, indicating that the overall elastoplastic deformation is rather rate-insensitive. The reduced modulus and the hardness are about 118 and 8.2 GPa, respectively, for all the loading rates studied.

TABLE I. Chemical composition of the Al-5%Mg (weight %).

Mg	Fe	Si	Ti	Mn	Cr	Zn	Zr	Al
4.7	0.01	0.01	0.005	0.001	0.001	0.001	0.001	Bal.

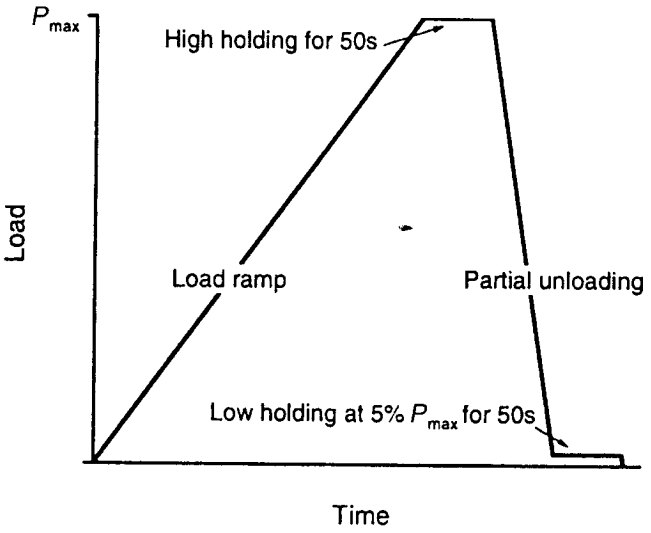

FIG. 2. Schematic illustration of the typical indentation sequence.

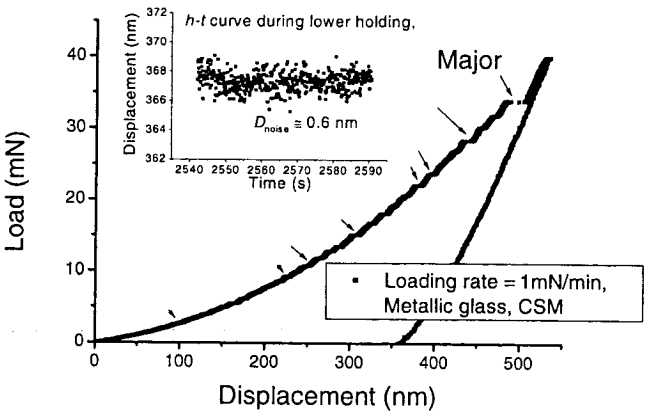

FIG. 3. *P–h* curve during indentation of metallic glass, showing a series of minor or major displacement bursts. The inset is the displacement–time curve obtained during low holding at a very small load.

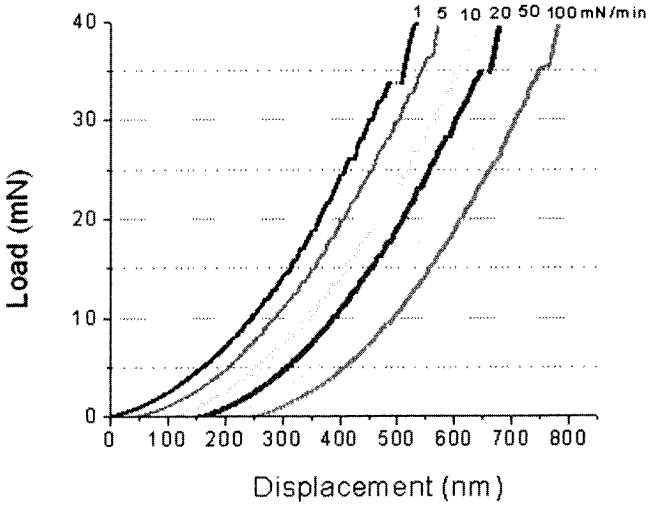

FIG. 4. Representative loading (P–h) curves of metallic glass under different loading rates. The origins of the curves are offset to show the difference between the curves.

The random strain bursts were quantified by subtracting the average elastoplastic behavior from the experimental data. To do this, the raw displacement (h) versus load (P) data were first fitted with a smoothing equation of the form

$$h = aP + bP^{1/2} + cP^{1/4} + d \quad , \tag{2}$$

where a to d are fitting constants. Figure 5(a) shows an example in the metallic glass, from which it can be seen that the fit using Eq. (2) is rather satisfactory. The upper panel of Fig. 5(b) shows the net difference between the raw data and the fitted curve during a typical section of the nanoindentation deformation in metallic glass, from which strain bursts are clearly seen as sudden displacement jumps of the order of a few nanometers. On top of the strain bursts due to deformation, oscillations with much higher frequencies but much smaller amplitudes due to machine noises are also seen in the upper panel of Fig. 5(b). To minimize the effect of noise, the raw data, after being utilized for the curve fitting according to Eq. (2), were then smoothened by a Savitzky–Golay filter.[13] The net difference between the smoothened data and the fitted curve is shown in the lower panel of Fig. 5(b), from which the starting points and end points of the bursts can be identified easily, and are marked as crosses and squares in Fig. 5(b). The upper panel of Fig. 5(c) shows the plot of the sizes of the displacement jumps ($\Delta h = h - h_{\text{fit}}$) versus the indentation depths h at which the jumps occur during loading of the metallic glass. It is obvious that the jump size Δh exhibits an increasing trend with h, on top of random fluctuations. However, a normalized quantity $\Delta h/h$, plotted in the lower panel of Fig. 5(c), exhibits no rising trend with respect to h, but only random fluctuations. In fact, since bursts in *strain* rather than in *displacement* are the concern here, the characterizing quantity should be dimensionless, and this is why $\Delta h/h$ should be a better measure of the size of the strain burst than Δh alone. Figure 5(d) shows the statistical distribution of $\Delta h/h$ from the metallic glass sample in double-logarithmic scale. It can be seen that the burst data appear to exhibit linear trend on the double-logarithmic scale, corresponding to the SOC power-law relation in Eq. (1). However, the small bursts at the slowest loading rate of 1 mN/min clearly deviate from linearity. Figure 5(e) shows the same set of data plotted in the semi-logarithmic scale, and apparent linear trends, corresponding to an exponential distribution of the form

$$F(\Psi) = ke^{-k\Psi} \quad , \tag{3}$$

are also apparent. The small bursts at 1 mN/min also seem to be better described by Eq. (3) as shown in Fig. 5(e) rather than Eq. (1) as shown in Fig. 5(d). However, due to the limited range of the burst sizes encountered in the present experiment, it is not possible to conclude unambiguously from Fig. 5(d) and 5(e) whether the SOC power law in Eq. (1) or the exponential form in Eq. (3) actually better describes the bursts in metallic glass.

Loading rates higher than 100 mN/min were also used in the present study, but the data were discarded. This is because the data acquisition rate is fixed at 10 points per second in the CSEM nanoindentation system used, and at such an acquisition rate, the sampling frequency is in the range of 1 point per 20 nm to about 1 point per 2 nm at a loading rate of 300 mN/min, for example. As can be seen from Fig. 5(b), such a low sampling frequency in the displacement domain is insufficient to reveal the bursts even if they really exist.

B. Amorphous selenium

To illustrate a totally different behavior, we look at the plastic flow of amorphous selenium. At room temperature, selenium undergoes viscoplastic deformation with very smooth P–h curves, a typical example of which is shown in Fig. 6(a). Figure 6(b) shows the difference between the raw displacement data and the fitted curve during a typical section of the deformation cycle, and when compared with Figure 5(b) for the case of metallic glass, strain bursts cannot be unambiguously identified in amorphous selenium, and only high-frequency, low-amplitude machine noises are observed. In other words, no strain bursts can be detected in amorphous selenium using the present nanoindentation technique.

C. Crystalline metals

All the crystalline metals studied exhibited continuous bursts in the nanometer scale. Figure 7(a) shows a typical

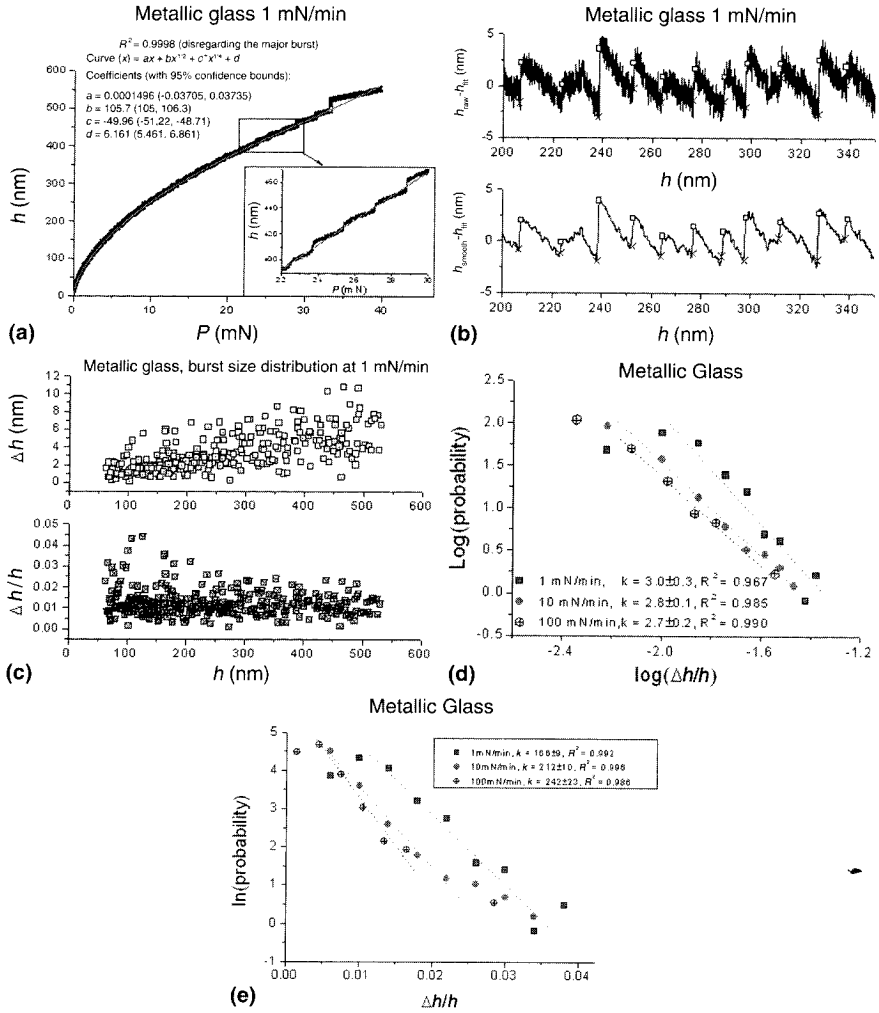

FIG. 5. (a) Typical displacement-load plot from metallic glass showing the raw data and the fitted curve using Eq. (2). Inset is an enlarged portion. (b) Identification of the starting and ending points of the strain bursts in metallic glass. Upper panel shows the difference between the raw displacement data and the fitted curve during a typical period of nanoindentation deformation in metallic glass. The lower panel shows the difference between the smoothed displacement data and the fitted curve, and the crosses and squares mark the strain-burst starting and ending points respectively. The size of each burst is calculated as the ending value minus the starting value. (c) Δh and $\Delta h/h$ versus h plots for metallic glass during loading at 1 mN/min. (d) Log(probability density) versus log($\Delta h/h$) plots in metallic glass during loading at various rates. (e) Semi-logarithmic plots of probability density of $\Delta h/h$ in metallic glass during loading at various rates.

loading curve observed from the Al-Mg alloy sample, from which intermittent bursts can be seen. Figure 7(b) shows the probability density profiles of $\Delta h/h$ at three different loading rates. It can be seen that for log($\Delta h/h$) smaller than ~2, the probability density is almost constant, but for log($\Delta h/h$) larger than ~2, the burst sizes appear to follow the power-law distribution in Eq. (1). The fitted SOC exponent k at different loading rates is approximately constant within the burst range encountered. Figure 7(c) shows the same set of data plotted in the semi-logarithmic scale. It can be seen that the data for small bursts seem to be better fitted by the exponential law in Eq. (3) than by the power law in Eq. (1). However, the large bursts seem to deviate from the exponential law behavior and indeed as shown in Fig. 7(b), they are better fitted by the power-law behavior.

The other crystalline metals studied also exhibit strain bursts with a spectrum of sizes. Figure 8 shows the flow behavior in the intermetallic compound Ni_3Al. As shown in Fig. 8(a), although the plastic loading curve appears to be smooth on a low-resolution scale, close inspection at a magnified view of any portion of the curve reveals random bursts of various sizes. Figure 8(b) shows the double-logarithmic plots of the probability density variation of the burst size $\Delta h/h$ at different loading rates. The plots in Fig. 8(b) clearly exhibit continuously changing slope, indicating that the experimental data cannot be described satisfactorily by the power-law relation in Eq. (1). However, the same data exhibit much clearer linear trends when plotted in a semi-logarithmic format as in Fig. 8(c). This indicates that the data are much better described by the exponential distribution in Eq. (3).

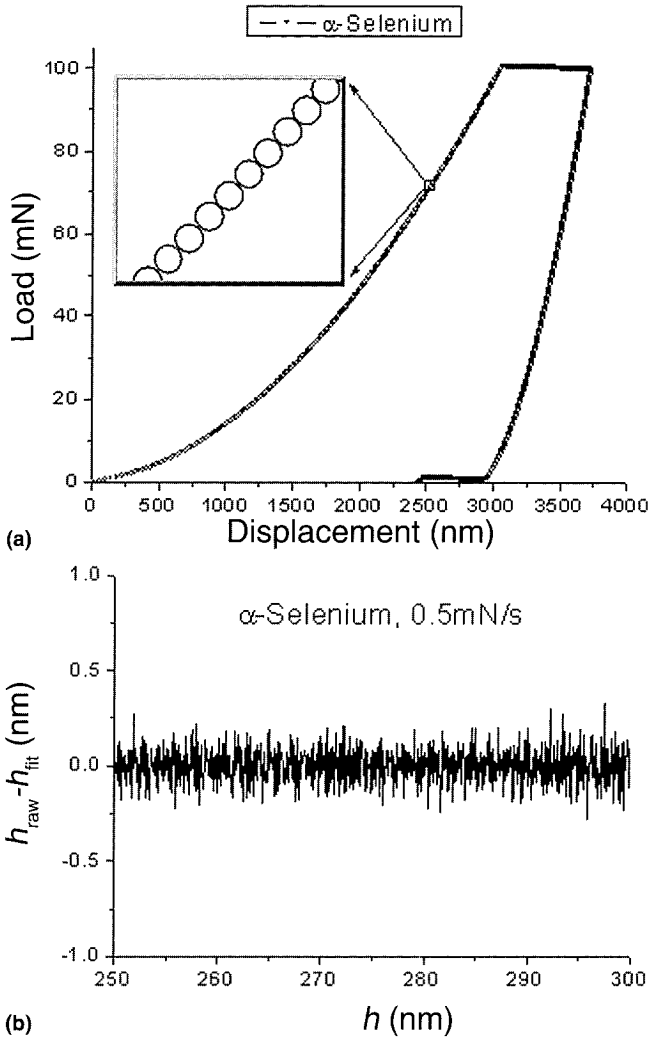

FIG. 6. (a) Indentation P–h curve in amorphous selenium at 20 °C. The inset demonstrates the smooth flow all through the indentation test. (b) Difference between the raw displacement data and the fitted curve versus h during loading in amorphous selenium at 20 °C. Only machine noise is detectable, and no strain bursts are observed.

The burst behaviors of copper, aluminum, zinc, and niobium are very similar to that of Ni_3Al. The loading curves of these materials all consist of random bursts on a nanometer scale. Figures 9(a) and 9(b) show respectively the double-logarithmic and semi-logarithmic plots of the probability density of the burst size $\Delta h/h$. The burst distributions in all these metals are better described by the exponential form in Eq. (3) rather than the power-law scaling behavior in Eq. (1).

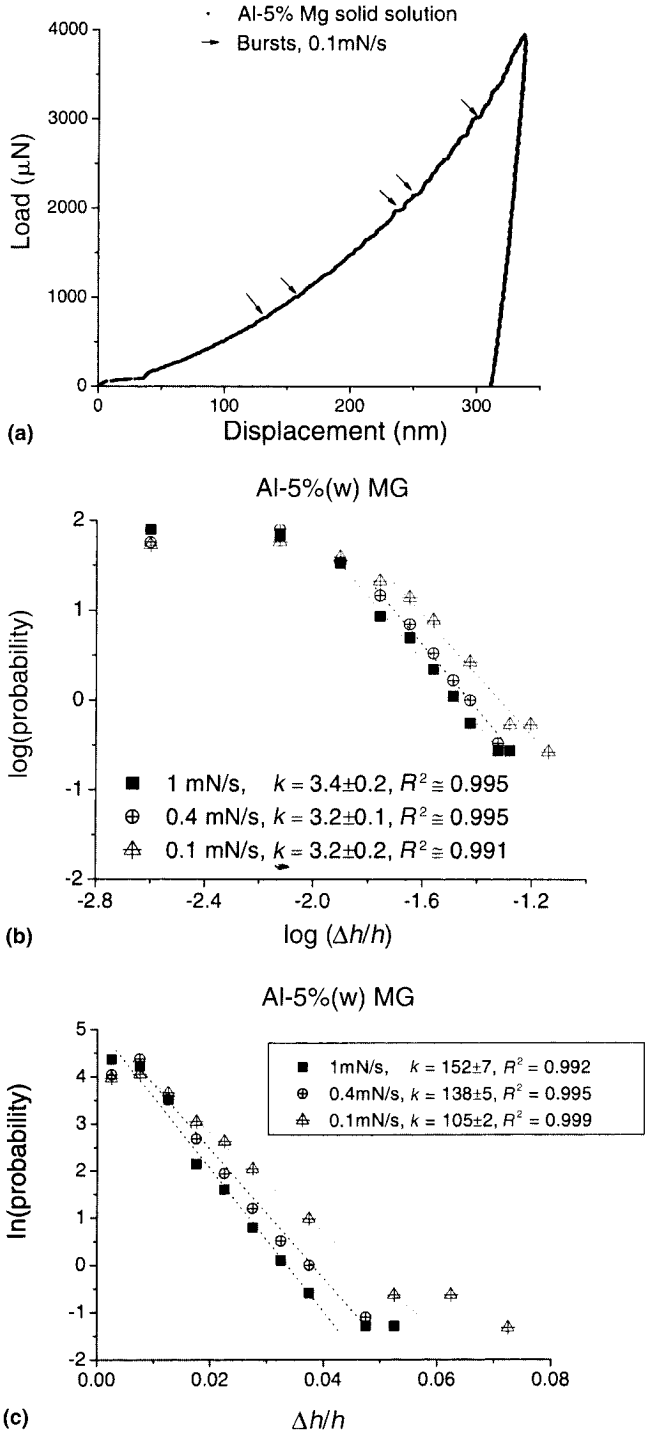

FIG. 7. (a) Indentation P–h curve in Al-5%Mg alloy at 0.1 mN/s loading rate. Curves obtained at different loading rates exhibit very similar overall responses. (b) Log(probability density) versus log($\Delta h/h$) plots in Al-5%Mg alloy during loading at various rates. (c) Semi-logarithmic plots of probability density of $\Delta h/h$ in Al-5%Mg alloy during loading at various rates.

IV. DISCUSSION

In this work, nanoindentation is used to quantify and characterize the continuous strain bursts during plastic deformation of a few representative materials. If indentation is performed with a pyramidal or conical indenter, the average stress and strain fields in the sample evolve in a self-similar manner. When the self-similar stress field propagates through the specimen, every material point in the specimen will eventually experience the

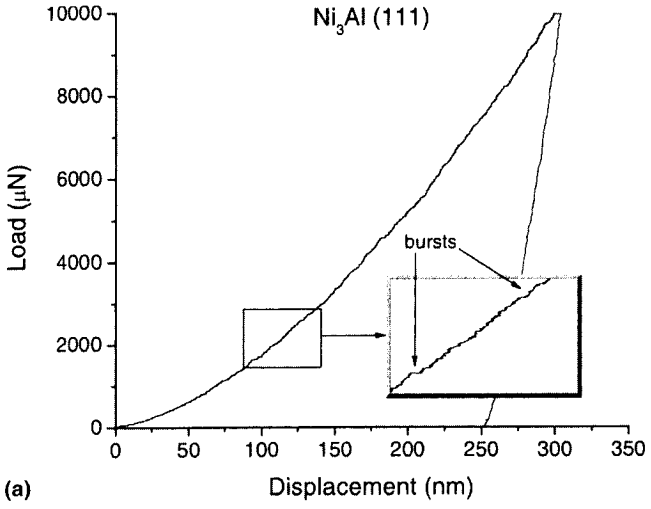

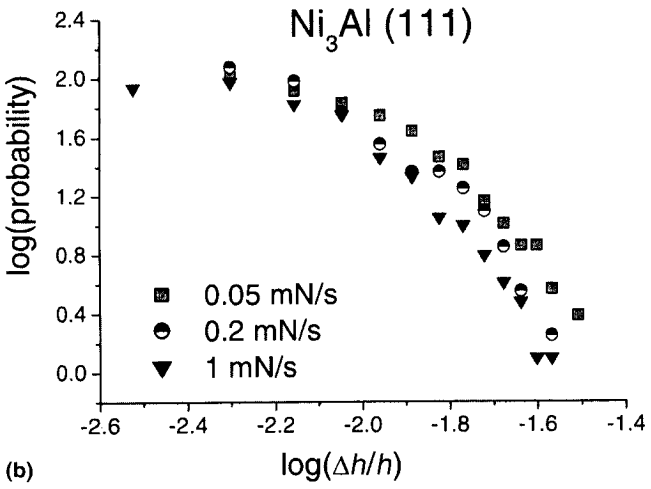

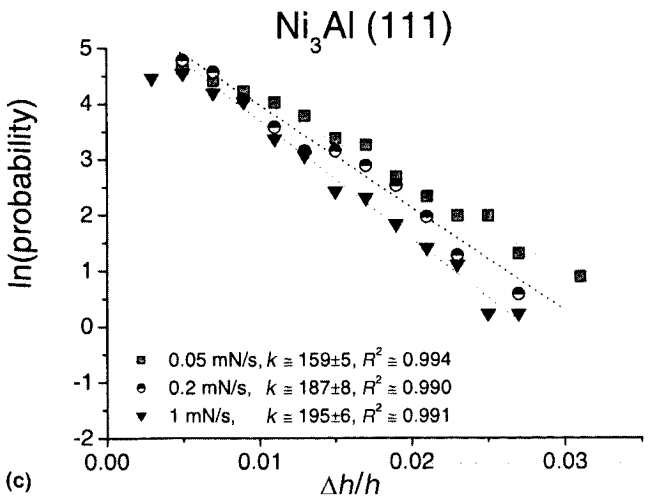

FIG. 8. (a) Indentation P–h curve in $Ni_3Al(Cr)$ (111) single crystal, and the inset demonstrates the presence of the intermittent bursts. (b) Log(probability) – log($\Delta h/h$) plots at different loading rates in $Ni_3Al(Cr)$. (c) Semi-logarithmic plots of probability density of $\Delta h/h$ at different loading rates in $Ni_3Al(Cr)$.

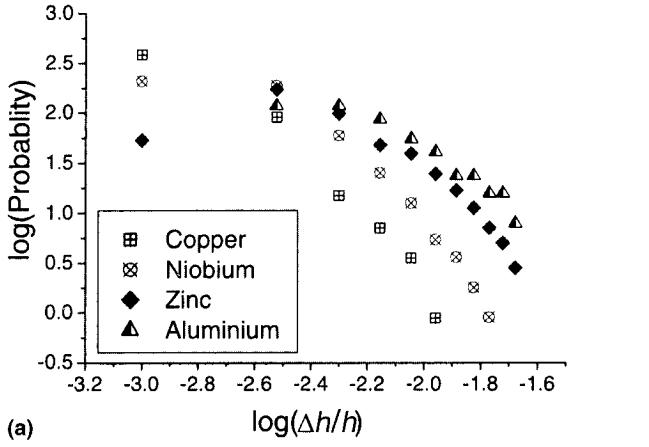

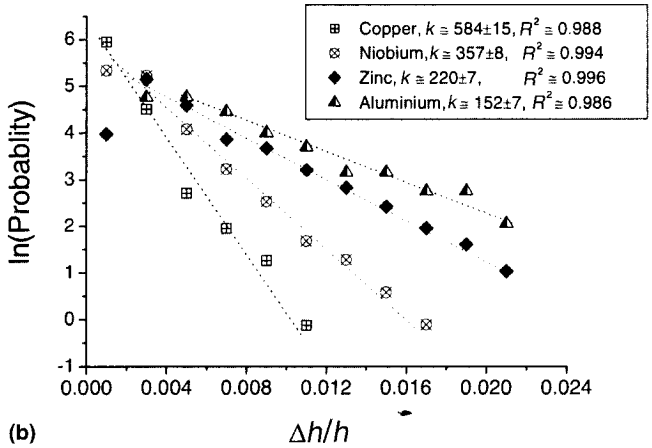

FIG. 9. (a) Log(probability) – log($\Delta h/h$) plots for copper, aluminum, zinc, and niobium. Loading rates and peak loads used: 30 mN/min to 30 mN for Cu; 1.7 mN/min to 2 mN for Al; 20 mN/min to 30 mN for Zn; 10 mN/min to 10 mN for Nb. (b) Semi-logarithmic plots of probability density of $\Delta h/h$ for copper, aluminum, zinc, and niobium. Same data as in (a).

same average stress path, although a time lag in general exists between one point and another. Thus, the strain bursts statistics observed from a nanoindentation experiment should represent the bulk situation at a stress which is some representative stress underneath the indenter. In particular, the analysis by Bower et al.[14] shows that the stress field $\underline{\sigma}(\vec{r})$ and the strain-rate field $\underline{\dot{\epsilon}}(\vec{r})$ scale as

$$\underline{\sigma}(\vec{r}) \sim \frac{P}{h^2}\,\underline{\Sigma}(\vec{r}/h) \quad \text{and} \quad \underline{\dot{\epsilon}}(\vec{r}) \sim \frac{\dot{h}}{h}\,\underline{\mathrm{E}}(\vec{r}/h) \quad , \qquad (4)$$

respectively, where $\vec{r}$ is the field point, P the indentation load, h the indentation depth, and $\underline{\Sigma}$ and $\underline{\mathrm{E}}$ are dimensionless tensor functions independent of P or h. Although these two scaling relations were derived for the case of constitutive power-law, rate-dependent deformation, we assume here that a scaling relation similar to the second relation in Eq. (4) can also approximately describe the strain rate produced by a local strain burst. In this case, the reciprocal of the function $\underline{\mathrm{E}}$ will be a Green's function relating a local event at $\vec{r}$ to a displacement response at

the sample free surface. Because $P \propto h^2$ during deformation, Eq. (4) suggests that if a strain burst of magnitude $\Delta\epsilon$ happens at $\vec{r}_1$ causing a sudden depth change Δh_1 when the indentation depth is h_1, then in a new situation with another indentation depth h_2, we can find a corresponding point $\vec{r}_2 = (\vec{r}_1/h_1) \times h_2$ which experiences the same stress as the burst point in the h_1 situation, and hence would have the same probability to produce a strain burst of the same magnitude $\Delta\epsilon$, and furthermore, $\Delta h_2/h_2 = \Delta h_1/h_1$. In other words, iso-stress locations in different indentation load or depth situations should have the same probability to produce a given magnitude of strain burst, with the same overall quantity $\Delta h/h$. This explains why the quantity $\Delta h/h$ can serve as an indicator for the strain burst, as experimentally observed in Fig. 5(c).

A range of different materials was selected in the present work in an attempt to reveal the effects of material structure. The deformation of amorphous selenium was found to be smooth with no unambiguous bursts. This is not surprising, as room temperature is already a very high homologous temperature compared to the glass transition temperature of about 35–40 °C,[15] and so deformation at this temperature is likely to occur by bulk viscous flow, which should be very smooth with little discrete internal obstacles. On the other hand, serrated flow is a well-known phenomenon in metallic glass at room temperature, and is thought to be due to the operation of shear bands in the amorphous structure.[8–12] The Portevin–Le Châtelier serrated flow phenomenon has also been reported previously to occur during nanoindentation of Al-Mg alloy.[16–19] The bursts in solid-solution alloys are thought to be related to the free-flight motion of dislocations between anchoring events at obstacles.[20] Dislocation motion in Ni_3Al and body-centered-cubic Nb are subjected to frequent thermal barriers, in the form of strong locks[21,22] and kink-pair barriers,[23,24] respectively. In Ni_3Al, in situ transmission electron microscopy experiments actually revealed discrete dislocation jumps of variable distances.[25] In conclusion, strain bursts in these materials are therefore well within expectation, and indeed, the present experiments successfully reveal them.

An important observation from the present experiments is that the bursts in the crystalline metals and alloys are found to be better described by the exponential law rather than the SOC power law. Due to the limited range of the burst sizes encountered in the present experiment, the bursts in the metallic glass cannot be concluded unambiguously to obey the exponential law, but such a possibility cannot be ruled out. The results here seem to contradict the acoustic emission experiments on ice crystals by Miguel et al.,[4] who revealed the SOC power-law behavior. The varying stress field underneath an indenter should not be an artificial factor to suppress the occurrence of an overall SOC behavior even though the "intrinsic," constant-stress behavior is SOC. This is because an "intrinsic" SOC behavior has no mean burst size to correspond to any "far-field" stress, and so there is also no mean burst size even though the stress field is non-uniform. However, there are other fundamental differences between nanoindentation and a macroscopic setting which must be considered when making a comparison. In Ref. 4, the majority of the strain bursts detected by acoustic emission in ice were of the order of 10^{-5} or 0.001%. In the present experiments, the strain bursts $\Delta h/h$ detected by nanoindentation as shown in Figs. 5, 7, 8, and 9 range typically from 0.5% to 2%. The reason for the much higher strain burst amplitudes in the nanoindentation setting is likely a result of the micron-scale strained volume. A single dislocation with a Burgers vector of typically 3 Å traveling over a distance of the order of one micron, which is roughly the size of the strained volume under the indenter, produces a strain increment of about 0.03%. Thus, each of the smallest strain bursts with magnitude 0.5–2% corresponds to the collective activities of only a few dozens of traveling dislocations. On the other hand, the strain produced by one single dislocation in a macroscopic sample in the acoustic emission experiment is many orders of magnitude smaller, and hence even the much smaller strain burst of size ~0.001% as detected by the acoustic emission technique represents the collective effect of many more moving dislocations than the nanoindentation situation. Owing to the very small size of the strained volume, the nanoindentation technique is therefore able to reveal large local deformations obtained from the motion of a very small number of individual dislocations, whereas the acoustic emission technique reveals small deformations obtained from the collective motion of a large number of dislocations.

The small size of the strained volume is probably the reason why the present results are better fitted by an exponential law rather than an SOC power law. The scale-free SOC behavior is generally believed to arise from interactions of a very large number of objects, giving bursts of any amplitude. On the contrary, the nanoindentation situation is concerned with the motion of a limited number of dislocations in a limited volume, and hence is characterized by a specific scale. This characteristic scale can be expressed in terms of a characteristic strain amplitude. Unlike the SOC power-law distribution which is free of any characteristic size, the exponential distribution in Eq. (3) is associated with a mean size given by $\langle\Psi\rangle = \int_0^\infty \Psi F(\Psi) d\Psi = 1/k$, where k is the exponent in the distribution. From the fitted values of k in Fig. 8(c) for Ni_3Al, for example, the mean strain burst size falls between 0.5% and 0.6% for the range of the loading rates studied. Similarly, the mean strain burst sizes in the other metals are 0.8–1.1% in Al-Mg, ~0.2% in Cu, ~0.3% in Nb, ~0.5% in Zn, and ~0.7% in Al. It is interesting to note that these characteristic strain

amplitudes again correspond to the motion of a few dozens of dislocations across the strained volume. In other words, it makes sense to attribute the loss of the SOC behavior in the nanoindentation situation to the micrometer-sized strained volume.

As discussed above, there are valid reasons why bursts can occur in the crystalline metals and alloys, and the metallic glass samples studied in this work. On the other hand, the rather generic observation of the exponential distribution of strain bursts from such a wide variety of materials with different structures indicates that the strain burst distribution is not strongly tied to the details of the deformation mechanism, which is very different among the different materials studied in this work. We believe that the exponential distribution of bursts is simply a consequence of balance between noise,[6,7] and the regulating factor imposed by the necessity to satisfy the characteristic burst size. We note that the exponential distribution corresponds to maximum entropy, or likelihood, at a given mean burst size. The situation is analogous to the statistical thermodynamics of an ideal gas, in which the Maxwell–Boltzmann energy distribution, which is also exponential, corresponds to maximum entropy for a given mean energy. Mathematically, the logarithm of the number of microscopically indistinguishable ways of arranging a sequence of bursts $\{\Psi_1, \Psi_2, \Psi_3, \ldots\}$ exhibiting an overall statistical distribution $P(\Psi)$is given by the Shannon entropy function[26]

$$S = -\int_0^\infty P(\Psi)\ln[P(\Psi)]d\Psi \quad . \qquad (5)$$

The distribution with maximum likelihood, under a given mean burst size, is then obtainable by maximizing the entropy functional in Eq. (5) subject to the constraint $\langle\Psi\rangle = \int_0^\infty \Psi F(\Psi)d\Psi$ = constant. Using standard variational calculus procedures, the result is the exponential distribution in Eq. (3), with the exponent given by $k = 1/\langle\Psi\rangle$, as we noted above. We therefore conjecture that the exponential distribution is observed in a wide range of materials in the present work because this is the most likely distribution to meet a certain mean burst size.

Finally, the case of the Al-Mg alloy with the Portevin–Le Châtelier effect needs further consideration. This alloy system is associated with a negative strain rate sensitivity that favors instabilities with large local strain rates. This is achieved through motion of relatively large density dislocation groups, enhancing the mutual elastic coupling between moving dislocations, and bringing the system closer to SOC conditions. As shown in Fig. 7, the observed burst amplitudes are in this case about 4 times larger than the pure metal cases in Fig. 9, i.e., 4 times as many dislocations are involved in the bursts. This is probably the reason why the large-magnitude data deviate from the exponential fit on the right of Fig. 7(c). Data are indeed better fitted in this case by a power law as in Fig. 7(b). For the same reason, the plateau evidenced on the log–log plot in Fig. 7(b) at small amplitudes is probably related to the fact that these extremely small events do not involve enough dislocations for SOC conditions to be fulfilled. The plateau region in fact corresponds to burst amplitudes of the order of those that can be fitted well by the exponential form in Figs. 8 and 9, i.e., involving only a few dozens of dislocations.

V. CONCLUSIONS

The nanoindentation technique was applied to investigate the scaling behavior of strain bursts during plastic flow in a range of materials, including a metallic glass, amorphous selenium, Ni_3Al, Al, Cu, Zn, Nb, and an Al-5%Mg alloy. The load-displacement data during constant-rate loading were analyzed to produce statistical information about the continuous strain bursts during deformation. Amorphous selenium during deformation at room temperature exhibited no detectable strain bursts. All the other materials studied exhibited random bursts of the nanometer scale. The probability distribution of the sizes of the strain bursts in Ni_3Al, Al, Cu, Zn, Nb, and Al-Mg is found to be better described by an exponential law rather than a power law as in self-organized criticality. In the metallic glass sample, the range of the burst sizes encountered does not enable definite conclusion on whether the power-law or the exponential-law behavior is obeyed. The absence of the self-organized critical behavior is likely a result of the small size of the strained volume in the nanoindentation situation, which gives rise to the constraint of a characteristic strain. Within the concept of Shannon's entropy, the exponential distribution is the most likely distribution at a given mean burst size, and this is thought to be the reason why a wide range of materials with very different internal structures can exhibit the same exponential distribution.

ACKNOWLEDGMENTS

We are grateful to Tang Bin for supplying nanoindentation data from selenium. We also thank Dr. S.H. Shek and Prof. B.J. Duggan for supplying the metallic glass and the Al-Mg samples. The work described in this paper was supported by grants from the Research Grants Council of the Hong Kong Special Administrative Region, China (projects HKU7201/03E and HKU7194/04E). We are grateful to an anonymous referee for pointing out several important differences between our nanoindentation experiments and a typical acoustic emission experiment.

REFERENCES

1. P. Bak, C. Tang, and K. Wiesenfeld: Self-organized criticality: An explanation of $1/f$ noise. *Phys. Rev. Lett.* **59,** 381 (1987).

2. P. Bak: *How Nature Works* (Springer-Verlag, Berlin, Germany, 1996).
3. J.Th.M. De Hosson, G. Boom, U. Schlagowski, and O. Kanert: Solution hardening in Al-Zn alloys. *Acta Metall.* **34,** 1571 (1986).
4. M.-C. Miguel, A. Vespingnani, S. Zapperi, J. Weiss, and J.-R. Grasso: Intermittent dislocation flow in viscoplastic deformation. *Nature* **410,** 667 (2001).
5. P. Häfner, K. Bay, and M. Zaiser: Fractal dislocation patterning during plastic deformation. *Phys. Rev. Lett.* **81,** 2470 (1998).
6. M. Zaiser, K. Bay, and P. Häfner: Fractal analysis of deformation-induced dislocation patterns. *Acta Mater.* **47,** 2463 (1999).
7. A.H.W. Ngan: Dislocation patterning—A statistical mechanics perspective. *Scripta Mater.* **52,** 1005 (2005).
8. Yu.I. Golovin, V.I. Ivolgin, V.A. Khonik, K. Kitagawa, and A.I. Tyurin: Serrated plastic flow during nanoindentation of a bulk metallic glass. *Scripta Mater.* **45,** 947 (2001).
9. T.G. Nieh, C. Schuh, J. Wadsworth, and Y. Li: Strain rate-dependent deformation in bulk metallic glasses. *Intermetallics* **10,** 1177 (2002).
10. C.A. Schuh, T.G. Nieh, and Y. Kawamura: Rate dependence of serrated flow during nanoindentation of a bulk metallic glass. *J. Mater. Res.* **17,** 1651 (2002).
11. C.A. Schuh, A.S. Argon, T.G. Nieh, and J. Wadsworth: The transition from localized to homogeneous plasticity during nano-indentation of an amorphous metal. *Philos. Mag.* **83,** 2585 (2003).
12. C.A. Schuh and T.G. Nieh: A nanoindentation study of serrated flow in bulk metallic glasses. *Acta Mater.* **51,** 87 (2003).
13. A. Savitzky and M.J.E. Golay: Smoothing and differentiation of data by simplified least squares procedures. *Anal. Chem.* **36,** 1627 (1964).
14. A.F. Bower, N.A. Fleck, A. Needleman, and N. Ogbonna: Indentation of a power law creeping solid. *Proc. R. Soc. London, Ser. A* **441,** 97 (1993).
15. B. Tang and A.H.W. Ngan: Measurement of viscoelastic properties of amorphous selenium using depth-sensing indentation. To appear in *Soft Mater.* **2,** 125 (2005).
16. Yu.I. Golovin, V.I. Ivolgin, and M.A. Lebedkin: Unstable plastic flow in the Al-3%Mg alloy in the process of continuous nanoindentation. *Phys. Solid State* **44,** 1310 (2002).
17. G. Bérces, J. Lendvai, A. Juhász, and N.Q. Chinh: Dynamic characterization of Portevin-Le Châtelier instabilities occurring in depth-sensing microhardness tests. *J. Mater. Res.* **18,** 2874 (2003).
18. W.A. Soer, J.Th.M. De Hosson, A.M. Minor, J.W. Morris, Jr., and E.A. Stach: Effects of solute Mg on grain boundary and dislocation dynamics during nanoindentation of Al-Mg thin films. *Acta Mater.* **52,** 5783 (2004).
19. N.Q. Chinh, J. Gubicza, Zs. Kovács, and J. Lendvai: Depth-sensing indentation tests in studying plastic instabilities. *J. Mater. Res.* **19,** 31 (2004).
20. Zs. Kovács, N.Q. Chinh, J. Lendvai, and G. Vörös: Portevin–Le Châtelier type plastic instabilities in depth sensing macro-indentation. *Mater. Sci. Eng.* **A325,** 255 (2002).
21. P.B. Hirsch: A model of the anomalous yield stress for (111) slip in $L1_2$ alloys. *Prog. Mater. Sci.* **36,** 63 (1992).
22. A.H.W. Ngan, M. Wen, and C.H. Woo: Atomistic simulations of Paidar–Pope–Vitek lock formation in Ni_3Al. *Comput. Mater. Sci.* **29,** 259 (2004).
23. A.H.W. Ngan and M. Wen: Dislocation kink-pair energetics and pencil glide in body-centered-cubic crystals. *Phys. Rev. Lett.* **87,** 075505 (2001).
24. D. Caillard and A. Couret: Dislocation movements controlled by friction forces and local pinning in metals and alloys. *Mater. Sci. Eng.* **A322,** 108 (2002).
25. G. Molenat and D. Caillard: Dislocation mechanisms in Ni_3Al at room-temperature—In situ straining experiments in TEM. *Philos. Mag. A* **64,** 1291 (1991).
26. C.E. Shannon: A mathematical theory of communication. *Bell Syst. Tech. J.* **27,** 379 & 623-656 (1948).